ACS chemical biology

Articles

pubs.acs.org/acschemicalbiology

Allosteric Competitive Inhibitors of the Glucose-1-phosphate Thymidylyltransferase (RmlA) from *Pseudomonas aeruginosa*

Magnus S. Alphey,[†,+] Lisa Pirrie,[†,‡,+] Leah S. Torrie,[§] Wassila Abdelli Boulkeroua,[†] Mary Gardiner,[§] Aurijit Sarkar,[§] Marko Maringer,[∥] Wulf Oehlmann,[⊥] Ruth Brenk,[§] Michael S. Scherman,[¶] Michael McNeil,[¶] Martin Rejzek,[#] Robert A. Field,[#] Mahavir Singh,[⊥] David Gray,[§] Nicholas J. Westwood,*[,†,‡] and James H. Naismith*[,†]

[†]Biomedical Sciences Research Complex, University of St. Andrews, St. Andrews KY16 9ST, U.K.

[‡]School of Chemistry, University of St. Andrews and EaStCHEM, St. Andrews KY16 9ST, U.K.

[§]Biological Chemistry and Drug Discovery, College of Life Sciences, University of Dundee, Dundee DD1 5EH, U.K.

[∥]mfd Diagnostics GmbH, Mikroforum Ring 5, 55234 Wendelsheim, Germany

[⊥]Lionex GmbH, Salzdahlumer Str. 196, 38126 Braunschweig, Germany

[¶]Department of Microbiology, Immunology and Pathology, Colorado State University, 1682 Campus Delivery, Ft. Collins, Colorado 80523-1682, United States

[#]Department of Biological Chemistry, John Innes Centre, Norwich NR4 7UH, U.K.

Supporting Information

ABSTRACT: Glucose-1-phosphate thymidylyltransferase (RmlA) catalyzes the condensation of glucose-1-phosphate (G1P) with deoxy-thymidine triphosphate (dTTP) to yield dTDP-D-glucose and pyrophosphate. This is the first step in the L-rhamnose biosynthetic pathway. L-Rhamnose is an important component of the cell wall of many microorganisms, including *Mycobacterium tuberculosis* and *Pseudomonas aeruginosa*. Here we describe the first nanomolar inhibitors of *P. aeruginosa* RmlA. These thymine analogues were identified by high-throughput screening and subsequently optimized by a combination of protein crystallography, *in silico* screening, and synthetic chemistry. Some of the inhibitors show inhibitory activity against *M. tuberculosis*. The inhibitors do not bind at the active site of RmlA but bind at a second site remote from the active site. Despite this, the compounds act as competitive inhibitors of G1P but with high cooperativity. This novel behavior was probed by structural analysis, which suggests that the inhibitors work by preventing RmlA from undergoing the conformational change key to its ordered bi-bi mechanism.

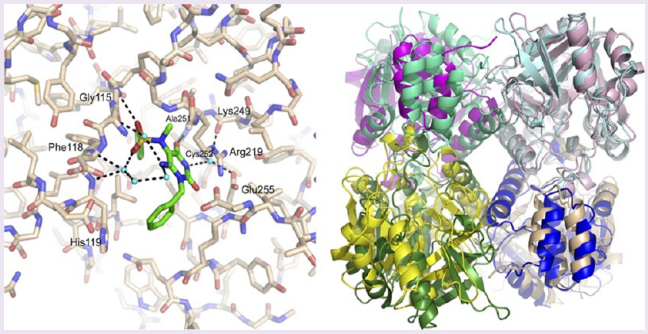

Pseudomonas aeruginosa is one of the most prevalent and opportunistic pathogens in hospital-acquired infections. It is a particularly difficult microorganism to treat due to its intrinsic chemo-resistance and its ability to acquire further resistance mechanisms against antimicrobial agents such as β-lactams, aminoglycosides, and fluoroquinolones.[1] The outer membrane of *P. aeruginosa* has low drug permeability properties,[2] and the species expresses a variety of efflux pumps.[3] The emergence of multidrug-resistant or even pan-resistant phenotypes of *Pseudomonas* means that even currently recommended combination therapies are less effective, having a negative impact on patient outcomes.[4] Currently, only a small number of novel anti-*Pseudomonal* drugs are in preclinical or clinical development, and very few have reached the market in recent years.[5] Although the World Health Organisation's recommended DOTS therapy (directly observed therapy, short course) is highly effective against *Mycobacterium tuberculosis*, one-third of the world's population is estimated to be infected, and the emergence of drug-resistant tuberculosis has been noted with alarm.[6,7] Development of novel antimicrobial compounds with new chemical scaffolds against novel enzyme targets is highly desirable.

The bacterial cell wall is a target for many antibiotics since it is vital for bacterial survival and is composed of peptidoglycans and lipopolysaccharides not found in eukaryotic cells. The biosynthesis of sugars in bacteria is in particular an important area of research (reviewed in ref 8). L-Rhamnose is part of the *O*-antigen of many Gram-negative bacterial cell wall lipopolysaccharides including *P. aeruginosa* but is not thought to be essential. In *M. tuberculosis* L-rhamnose links the

Received: August 15, 2012
Accepted: November 8, 2012
Published: November 8, 2012

   dx.doi.org/10.1021/cb300426u | *ACS Chem. Biol.* 2013, 8, 387–396

peptidoglycan to the arabinogalactan components, and genes associated with L-rhamnose biosynthesis have been shown to be essential in this microorganism.[9] dTDP-L-rhamnose is synthesized from glucose-1-phosphate (G1P) and deoxy-thymidine triphosphate (dTTP) by four enzymes. These enzymes are potential therapeutic targets, and inhibitors of the pathway enzyme RmlC are being investigated.[10−13] The first enzyme, glucose-1-phosphate thymidylyltransferase (RmlA), catalyzes the condensation of G1P with dTTP to give dTDP-D-glucose (Figure 1A).[14,15] RmlA is homologous to other bacterial sugar nucleotide transferases (*e.g.*, G1P uridylyltransferase[16]), though RmlA's tetrameric arrangement is distinct (Figure 1B). The tetramer can be thought of as a dimer of dimers. The dimer "building block" contains what we term the monomer−monomer interface, and the dimer−dimer interface links together the two dimers (Figure 1B). The inhibition of RmlA by dTDP-L-rhamnose, the final pathway product, has been reported to occur in both a competitive and noncompetitive manner.[17] The presence of this feedback mechanism suggests that RmlA is the point of control for the pathway. Based on sequence conservation and interactions with substrates, previous studies have identified the active site of RmlA as adjacent to the dimer−dimer interface.[15] Specifically, residues in loops 10−25, 138−148, and 224−232 are involved not only in forming the active site but also in subunit interactions. A second (or allosteric) site in RmlA was observed in two earlier studies[15,18] and found to bind thymidine-containing compounds at the monomer−monomer interface. In summary, each monomer has one active site completely enclosed by the monomer and one second site. The second site is some 20 Å distant from the active site and sits at the monomer−monomer interface, utilizing residues from both monomers.[15,18] RmlA has attracted considerable attention from a protein engineering standpoint and its use in so-called glycorandomization.[18−20]

The allosteric modulation of enzyme activity by small molecules, resulting in either activation or inhibition, has received considerable attention in recent years.[21−25] Allosteric inhibitors offer several advantages over traditional active site inhibitors as they generally exhibit a higher selectivity due to the allosteric site residues having conservation across a protein superfamily lower than that of the corresponding active site residues. Lower off target effects result from this and may lead to a decrease in inhibitor toxicity and side effects.[26] The mechanisms by which allosteric modulators exert their activity can shed light on enzyme mechanisms. In terms of kinase inhibition, the development of allosteric inhibitors that show selective isoform inhibition has proved possible in cases where selectively targeting the active site is challenging.[27] The identification of novel allosteric inhibitors, however, remains a considerable challenge.

To date no small molecule inhibitors of RmlA have been reported. Here, we report the discovery and optimization of a series of *Pseudomonas aeruginosa* RmlA inhibitors, several of which have nanomolar activity against the enzyme. Weak activity against *M. tuberculosis* has also been demonstrated. The inhibitors interact with RmlA in a highly cooperative manner with the inhibitor core structure mimicking the thymine ring of RmlA's substrate dTTP. The inhibitors bind only to the allosteric site on RmlA not at the active site.

RESULTS AND DISCUSSION

Identification of Initial Hits. *Pseudomonas aeruginosa* RmlA was screened against a diverse library of 15,667 compounds[28] at a single concentration of 30 μM using an assay that monitors phosphate levels.[29] Forty-three compounds displayed >30% inhibition (hit rate of 0.27%) and were designated potential hits. Retesting this set in duplicate as 10-point dose−response curves enabled IC_{50} value determination. Compounds **1** and **2** gave reliable data with IC_{50} values of 0.22

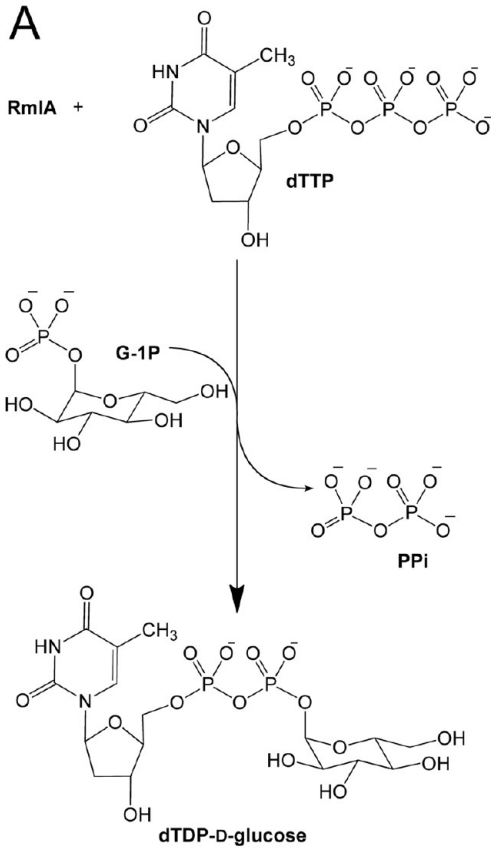

Figure 1. Enzymatic reaction and quaternary structure of RmlA. (A) Enzyme substrates dTTP and G1P are combined to produce dTDP-D-glucose and pyrophosphate. (B) Tetrameric arrangement of RmlA, with the four interacting subunits shown in different colors. The active and allosteric site positions are marked; there is one of each site per monomer. The active sites are located at the dimer−dimer interfaces but are formed by residues from only one monomer. The allosteric sites are located at the monomer−monomer interfaces and are formed by residues from both monomers.

Table 1. Inhibition Data against RmlA for Analogues of 1[a]

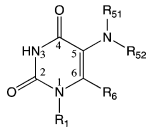

compound[b]	R_1	R_{51}	R_{52}	R_6	% inhibition at 10 μM[c]	% inhibition at 60 μM[c]	IC_{50} (μM)[d]
1	^{n}Bu	Me	SO_2Ph	NH_2	100	100	0.21 ± 0.03
2	benzyl	H	H	OH	100	85.7 ± 2.1	1.14 ± 0.19
3	^{n}Bu	Me	C(=O)Ph	NH_2	30.3 ± 4.1	75.7 ± 3.9	n.d.
4	^{n}Bu	H	cyclopentyl	NH_2	30.0 ± 2.0	39.4 ± 4.6	n.d.
5	^{n}Bu	Me	C(=O)-2-furan	NH_2	71.1 ± 1.2	100	5.9 ± 2.9
8a	benzyl	Me	SO_2Ph	NH_2	100	100	0.073 ± 0.01
8f	benzyl	Me	COPh	NH_2	0	14.5 ± 0.6	>60
15a	benzyl	H	SO_2Ph	NH_2	94.2 ± 0.8	100	1.32 ± 3.7
8b	benzyl	Et	SO_2Ph	NH_2	100	100	0.102 ± 0.02
8c	benzyl	^{n}Pr	SO_2Ph	NH_2	100	43.4 ± 2.3	>10
12a	benzyl	Me	H	NH_2	10.7 ± 3.7	3.1 ± 3.5	>60
12b	benzyl	Et	H	NH_2	97.8 ± 1.5	82.4 ± 1.9	4.7 ± 4.0
8j	benzyl	Me	SO_2-*n*-Bu	NH_2	100	100	0.175 ± 0.067
8k	benzyl	Me	SO_2-4-F-Ph	NH_2	100	100	0.205 ± 0.009
8p	benzyl	Me	SO_2-3-Me-Ph	NH_2	100	100	0.387 ± 0.065
8t	benzyl	Me	SO_2-2-furan	NH_2	100	100	0.105 ± 0.012

[a]For assay data relating to additional analogues see Table S7 in Supporting Information. [b]The following PDB codes are assigned to structures of the complexes of RmlA bound to **1** (4ARW), **2** (4AS6); **3** (4B42); **4** (4B2X); **8a** (4ASJ); **8f** (4ASY); **15a** (4ASP); **12b** (4B3U); **8j** (4B4G); **8k** (4B4M); **8p** (4B5B); for data collection and model refinement statistics for all RmlA-inhibitor complexes see Supporting Information. [c]SE, standard error (n = 2). [d]SD, standard deviation (n = 3).

μM (95% CI 0.18−0.27 μM) and 1.23 μM (95% CI 0.92−1.67 μM), respectively (Table 1 and Supplementary Figure S1). Both **1** and **2** gave large Hill coefficients (3.55 ± 0.25 for **1** and 1.75 ± 0.42 for **2**, Supplementary Figure S1). Isothermal calorimetry (ITC) gave a K_d = 0.074 ± 0.006 μM for **1** and K_d = 0.395 ± 0.02 μM for **2** (Supplementary Figure S2).

Structural Characterization of Initial Hits. Multiple crystal structures of substrate/product complexes of RmlA from *P. aeruginosa* have been reported.[15,18] RmlA crystals were soaked overnight with **1** or **2**, and clear density for four bound inhibitors was identified in the tetramer (Figure 2 and Supplementary Table S1). The inhibitor binding sites were not the active sites, rather the allosteric sites.[15] The allosteric site is predominantly hydrophobic in character and sits at an intersubunit interface formed by residues from two adjoining subunits of the tetramer: Tyr38, Ser41, Leu45, Tyr114, Gly115, Phe118, His119, Leu122, Val250, Ala251, Glu255, Ile256, Arg259 from one monomer and Gly218′, Arg219′ from the second monomer.

The pyrimidinedione core in **1** stacks against Arg219′ and forms hydrophobic interactions with Leu45 and Ile256 (Figure 2A and Supplementary Figure S3). The C4 carbonyl hydrogen bonds directly to Ala251N, and N3H interacts *via* a single water molecule with Lys249O, Cys252N, and Glu255OE1. These interactions directly match those previously observed in complexes of RmlA with the thymidine-containing compounds dTTP, dTDP, dTMP, dTDP-D-glucose, or dTDP-L-rhamnose bound at this allosteric site.[15,30] The C6-amino group interacts with two water molecules, one of which hydrogen bonds to Gly115O (Supplementary Figure S3). The C5-*N*-methylsulfonamide makes a hydrogen bond with Gly115N and a water-mediated hydrogen bond with Phe118N and His119N. In addition, the sulfonamide phenyl ring makes a face-edge hydrophobic interaction with the side chain of Phe118 and sits in a hydrophobic pocket surrounded by Leu45, Val250, Ala251, and Ile256 (Figure 2A). The N1-*n*-butyl chain of **1** packs against the side chain of Arg259 from a neighboring subunit. The pyrimidinetrione core of **2**, including the N3H and the C4 carbonyl, and the N1-benzyl substituent make essentially the same contacts with RmlA as described for **1** (Figure 2B and Supplementary Figure S4). In this structure with **2**, an additional glycerol molecule is bound in the equivalent position to the phenyl group of the C5-*N*-methylsulfonamide group in **1** (Supplementary Figure S5).

Commercial Analogues. A 2D-similarity screening approach was undertaken to identify commercially available analogues of **1** and **2**. Structural analysis suggested that the interactions of the central ring including the N3H and C4 carbonyl group would be crucial for binding to RmlA (Supplementary Figure S6). Commercially available analogues containing a pyrimidinedione or pyrimidinetrione ring system were identified, and 15 analogues were purchased and assayed (Table 1, Supplementary Tables S2 and S3). None of these compounds were more potent than **1**; however, these studies showed that replacement of the sulfonamide in **1** by an amide in **3** or an alkyl substituent in **4** was detrimental (Table 1). Replacement of the amide phenyl ring by a furan in **5** partially compensated for the loss in activity. Complexes with **3**, **4**, and **6** (Supplementary Table S4) showed that the central ring of these inhibitors remained in essentially the same position as **1**, with only minor angular distortions with respect to each other as a result of variations in stacking of N1-substituents with Arg259 (Supplementary Figure S7A). However, two of the compounds appear to react with the buffer at the central carbon of the 1,3-diketone functional group under the crystallization conditions (see analogues **6** and **7** in Supplementary Figures S7B and S7C).

dx.doi.org/10.1021/cb300426u | *ACS Chem. Biol.* 2013, 8, 387−396

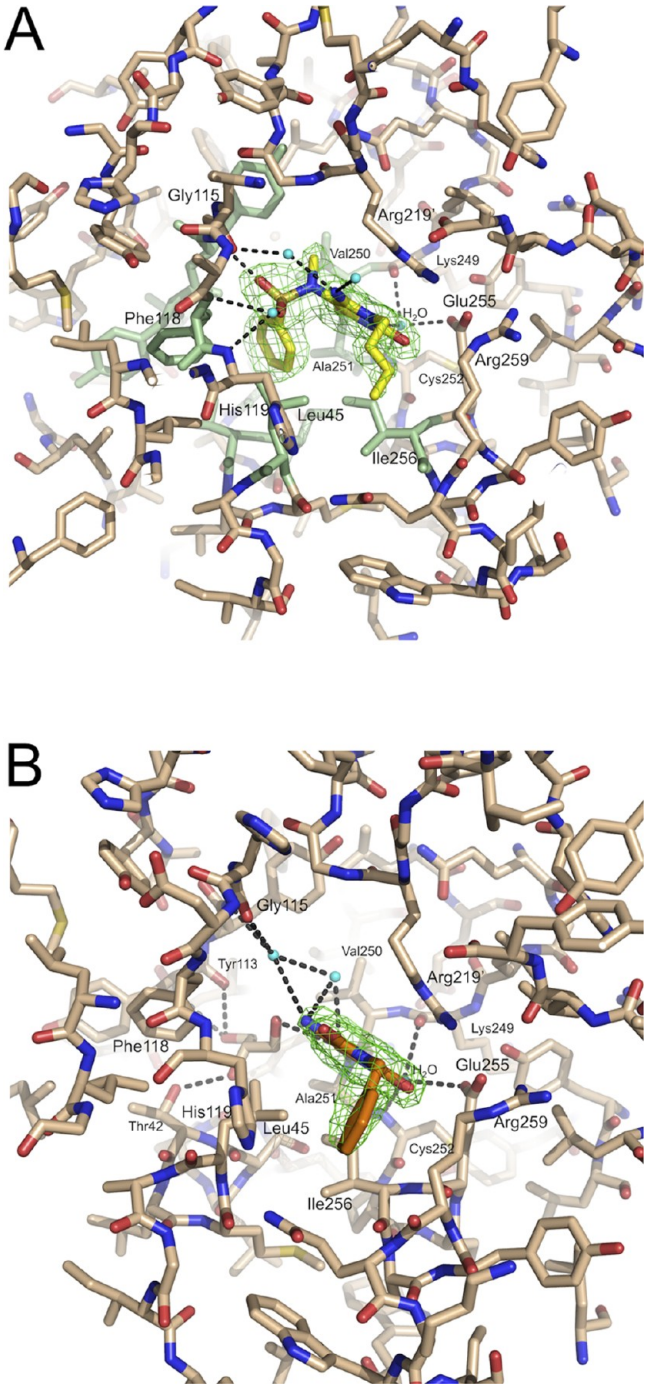

Figure 2. Representative stick images of RmlA crystal complexes with screening hits **1** and **2**. (A) RmlA-**1** complex. (B) RmlA-**2** complex. Both show omit (ligand removed, structure rerefined) $2F_o - F_c$ electron density maps (contoured at 1.2σ) and selected hydrogen bonds (black dotted lines) (PDB codes 4ARW and 4AS6). Important residues are highlighted with the sulfonamide binding region residues colored green in panel A. **1** is colored yellow, **2** orange, nitrogen atoms blue, oxygen atoms red, and water molecules cyan. Figures were prepared using PyMOL.[41] Further details of the binding of RmlA to **1** and **2** are shown in Supplementary Figures S3 and S4. Unbiased original $F_o - F_c$ maps are shown for all ligands in Supplementary Figure S19.

Synthesis of Analogues of 1. We synthesized inhibitor **8a**, the N1-benzyl analogue of **1** (Scheme 1 and Table 1), to explore the role of the N1 substituent more fully. Reaction of *N*-benzyl urea (**9**) with **10** led to the formation of the pyrimidinedione ring in **11**.[31] Selective C5-bromination of **11** enabled incorporation of the required methylamine functionality to give **12a**, which was subsequently converted to **8a** in good yield. Analogous methodology was used to prepare **8b−e** *via* the corresponding amines **12b−e** (Scheme 1) and a further 18 C5-N-sulfonamide analogues were prepared from **12a** (Table 1 and Supplementary Table S5 for structures). Reaction of **12a** with benzoyl chloride gave **8f**, the amide analogue of **8a**, whereas conversion of **11** to the corresponding nitroso-derivative **13** enabled the synthesis of analogues **14** and **15a,b**.

Analysis of Novel Analogues of 1. Replacement of the N1-*n*-butyl substituent in **1** with an N1-benzyl substituent in **8a**, a change inspired by the structure of **2**, led to a considerable increase in potency with **8a** having an IC_{50} of 0.073 ± 0.01 μM against RmlA (Table 1, entry 6) and a K_D of 0.028 ± 0.003 μM (Supplementary Figure S2). Superposition of the structures of the RmlA-**1** with RmlA-**8a** (Supplementary Figure S8 and Table S6) showed no change in the interaction made by the inhibitor core with the enzyme and almost identical positioning of the C5-*N*-methylsulfonamide substituent. The significant difference in potency between **8a** and **1** seems most likely to result from improved protein−ligand hydrophobic interactions in the N1-binding pocket (Supplementary Figure S8).

As in the N1-*n*-butyl series (cf. Table 1, entries 1 and 3), replacement of the sulfonamide substituent in **8a** by an amide proved detrimental (**8f**, entry 7). An overlay of the structure of RmlA-**8a** and RmlA-**8f** complexes showed that the contacts made between the enzyme and the pyrimidinedione rings of **8a** and **8f** were preserved (Supplementary Figure S9 and Table S6). However, binding of the amide in **8f** to RmlA resulted in a decrease in the hydrogen bonding network associated with the amide group compared to that present with the sulfonamide in **8a** (Figure 3A−D). In addition, the *N*-methylamide substituent in **8f** was forced to rotate by 50° compared to its position in the RmlA-**8a** complex with a corresponding 1.4 Å movement in the position of the methyl group. An analogous decrease in hydrogen bonding and rotation of the *N*-methyl substituent was also seen when the structures of the RmlA-**1** and RmlA-**3** complexes were compared (Supplementary Figure S10).

The *N*-methyl group in **8a** was shown to be important for inhibition of RmlA (cf. Table 1, entries 6 and 8) with the C5-NH analogue **15a** being 18-fold less potent than **8a**. The difference in potency between **8a** and **15a** was rationalized on the basis of the occupancy of a small hydrophobic pocket by the *N*-methyl group in **8a**. The top of the *N*-methyl pocket is lined by hydrophobic groups including Val250 and the methylene units of the Arg219′ side chain. Analysis of a series of *N*-alkyl analogues of **8a** showed that while an ethyl substituent was tolerated, a rapid drop off in potency was observed for longer alkyl chain lengths (**8b−e**, Table 1 and Supplementary Table S5). On replacement of the sulfonamide substituent by a hydrogen atom, only the C5-N-ethyl analogue **12b** inhibited RmlA (**12a−e**, Table 1 and Supplementary Table S5). Structural studies showed that in the RmlA-**12b** complex the C5-N-ethyl substituent no longer occupied the previously identified hydrophobic pocket but instead was positioned in a nearby cleft (Supplementary Table S7 and Figure S11).

To probe further the pocket occupied by the sulfonamide group in **8a**, a set of 18 analogues with varying sulfonamide groups was synthesized. In brief, replacement of the phenyl ring in the sulfonamide with an alkyl substituent was tolerated with **8j** inhibiting RmlA with an IC_{50} of 0.175 ± 0.067 μM (Table 1,

dx.doi.org/10.1021/cb300426u | ACS Chem. Biol. 2013, 8, 387−396

Scheme 1. Synthesis of Analogues of 1[a]

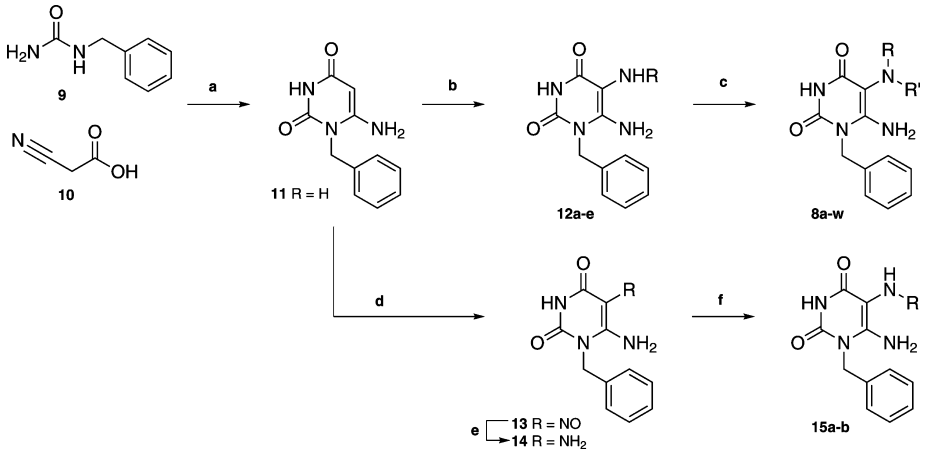

[a]Reagents and conditions: (a) Ac_2O, 80 °C, 2 h then 10% aq NaOH, 85 °C, 1 h, 51%;[31] (b) Br_2, $NaHCO_3$, MeOH, 0 °C to rt, 30 min then 30% aq amine, 70 °C, 4 h, 69% for **12a**; 30% (**12b**); 28% (**12c**); 11% (**12d**); 8% (**12e**); (c) for **8a**–**e** phenylsulfonyl chloride, pyridine, DCM, rt, 16 h, 65% for **8a**; 54% (**8b**); 54% (**8c**); 60% (**8d**); 51% (**8e**); 44–85% for **8g**–**w**; for **8f** benzoyl chloride, pyridine, DCM, rt, 16 h, 73%; (d) $NaNO_2$, AcOH/H_2O, 70 °C to rt, 1 h, 72%; (e) $Na_2S_2O_4$, NH_4OH, 6 h, 75%; (d) phenylsulfonyl chloride or benzoyl chloride, pyridine, DCM, rt, 26 h, 71% for **15a**; 75% for **15b**.

entry 13). Structural analysis of the RmlA-**8j** complex showed that hydrophobic interactions between the alkyl side chain and Phe118 were present (Supplementary Figure S12). Substitution in the phenylsulfonamide ring of **8a** was in general poorly tolerated with the exception of small groups at the 3- or 4-positions (Table 1 and Supplementary Table S5; see Supplementary Figure S13 for structural insights gained from analysis of the RmlA-**8k** and RmlA-**8p** complexes). Replacement of the phenyl ring with a 2-furan ring gave the potent inhibitor **8t** (IC_{50} of 0.105 ± 0.012 μM, Table 1, entry 16); however, exchange for a larger aromatic or heteroaromatic ring or a benzyl substituent was not tolerated (Supplementary Table S5).

Biological Data. *P. aeruginosa* PAO1, which had the RmlA gene knocked out, grew in culture normally but showed significantly reduced numbers of colonies in mouse lung after infection compared to wild type *P. aeruginosa* PAO1 (Supplementary Figure S14). This confirmed RmlA is not essential for survival but is important for virulence. In simple assays of bacterial growth (both plate and suspension), no compound exhibited inhibition of *P. aeruginosa* PAO1. Selected compounds (Supplementary Table S8) were tested against *M. tuberculosis*, for which RmlA is essential,[9] and compounds **8f** and **8p** showed MIC_{100} values of 25 and 50 μg mL^{-1}, respectively (the value for isoniazid is 0.078 μg mL^{-1}). We have as yet been unable to express RmlA from *M. tuberculosis* in sufficient quantity to assay the compounds *in vitro*.

Mode of Inhibition. To fully understand the enzyme reaction mechanism and mode of inhibition of compound **8a**, biochemical assays and surface plasmon resonance (SPR) methods were utilized. Initial biochemical experiments reveal the substrate Michaelis constants to be 7.8 μM (95% CI 4.3–14.4 μM) and 9.5 μM (95% CI 6.8–13.5 μM) for dTTP and G1P, respectively (Supplementary Figure S15). For both substrates the Hill coefficient was found to be ∼1, indicating no evidence of cooperativity within the tetrameric protein.

SPR experiments showed that dTTP binds to apo-RmlA with a K_D of 39.9 μM (95% CI 35.9–44.3 μM),whereas apo-RmlA does not bind G1P (Supplementary Table S9 and Figure S16). However, when each substrate was titrated in the presence of a fixed, saturating concentration of the second substrate, K_D values comparable to the Michaelis constants were measured (6.70 μM (95% CI 5.55–8.10 μM) for G1P and 6.02 μM (95% CI 5.03–7.20 μM) for dTTP) (Supplementary Table S9 and Figure S16). The binding of dTTP is therefore required to create a functional G1P binding site, consistent with the previously described[17,30] sequential ordered bi-bi mechanism of catalysis employed by RmlA (Supplementary Figure S16). Since both substrates are negatively charged, a simple charge–charge attraction can be ruled out. The most likely explanation is that dTTP binding triggers a conformational change in the protein that forms the G1P binding site.

As previously described, inhibitor **8a** was tested in the biochemical assay with an IC_{50} of 0.073 μM calculated. In addition to the biochemical studies, SPR experiments confirm **8a** binds to RmlA (Supplementary Figure S17). This SPR binding data could not be fitted to a 1:1 binding model, indicating **8a** binds to the RmlA tetramer with some level of cooperativity.

To investigate the mode of inhibition of **8a**, kinetic assays were performed. With G1P in excess and varying dTTP concentrations in the presence of different concentrations of **8a**, only weak (essentially no) inhibition of dTTP binding was observed until inhibitor concentrations were raised to around 400 nM, where almost complete inhibition occurred (Figure 4A). Using a saturating concentration of dTTP and varying the concentrations of G1P and **8a** showed that **8a** displayed competitive inhibition with respect to G1P (Figure 4B) (estimated K_i = 0.020 ± 0.020 μM). Analysis of these data shows a Hill slope of 3.6. These findings were confirmed using SPR, with no binding of G1P observed in the presence of 1 μM **8a** and a saturating concentration of dTTP (Figure 5 and Supplementary Table S9). Conversely binding of dTTP was observed when titrated in the presence of 1 μM **8a** and a saturating concentration of G1P (albeit with a reduced binding affinity compared to the K_D calculated in the absence of compound **8a**) (Figure 5 and Supplementary Table S9).

Given the SAR relationship of the compounds and the structural data that show they all bind in the same place, we conclude that our inhibitor series all act as competitive

dx.doi.org/10.1021/cb300426u | *ACS Chem. Biol.* 2013, 8, 387–396

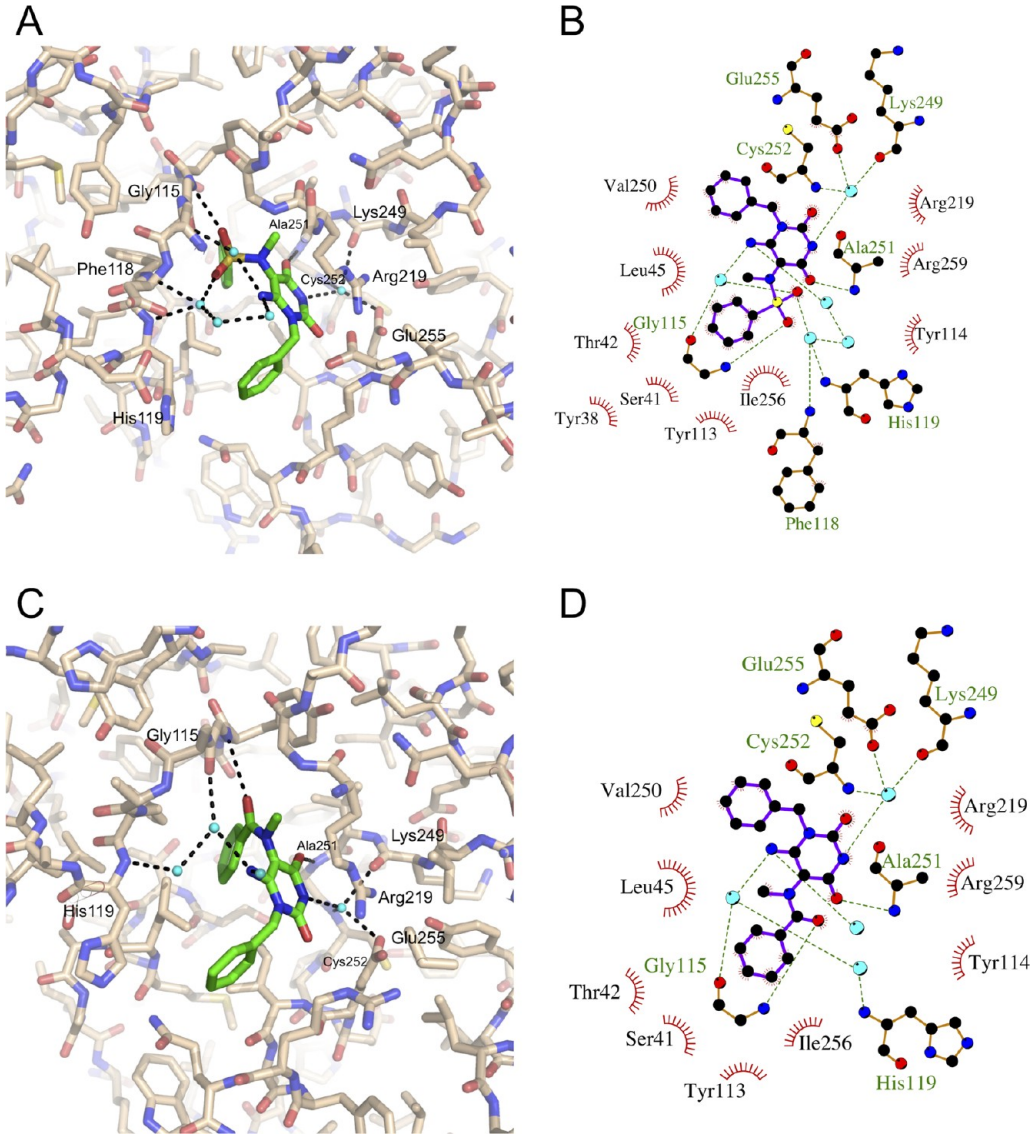

Figure 3. Crystal complexes of RmlA-**8a** and RmlA-**8f**. (A) **8a** bound in the allosteric site of RmlA. (B) Schematic representation of the key interactions present in the RmlA-**8a** complex. (C) **8f** bound in the allosteric site of RmlA. (D) Schematic representation of the key interactions present in the RmlA-**8f** complex. Hydrogen bonds are shown as black dotted lines in the stick figures and green dotted lines in the schematics.

inhibitors of G1P. ITC data for three compounds (**1**, **2**, and **8a**) correlate with the IC_{50} values, thus the tighter the binding the more potent the inhibitor. This is in contrast to common assumption that an inhibitor binding at a site remote from the active site would behave as a noncompetitive inhibitor. The potential for compounds binding at a second (allosteric) site to act as competitive, noncompetitive, or uncompetitive inhibitors is however known. dTTP, which binds at the allosteric site, weakly inhibits the enzyme (Supplementary Figure S18). dTDP-D-glucose, dTDP, and dTDP-L-rhamnose also bind at this site (all products in the dTDP-L-rhamnose pathway).[15] We determined IC_{50} for dTMP, dTTP, dTDP-glucose, and dTDP-L-rhamnose (Supplementary Table S10). We suggest that binding at this second site is the point of control of the rhamnose pathway; dTDP-L-rhamnose (as well as any intermediates on the pathway) shuts down RmlA thus regulating pathway flux.

We re-examined our structural and kinetic data to identify a molecular basis for this inhibition. It is interesting to note that the Hill slope for inhibitor **8a** (and many other hit compounds) is $\gg 1$, the expected value for a 1:1 binding relationship. Indeed the Hill slope for **8a** was calculated as 3.61 ± 0.04, which is approaching the theoretical maximum of 4 for the RmlA tetramer. This highly cooperative behavior is unusual, and we can find no comparable case of such high values for a tetramer (hemoglobin has a Hill coefficient of 2.8). Slopes of this magnitude imply the tetramer is either completely free from inhibitor or all four sites are occupied.

The RmlA active sites are located at the dimer−dimer interfaces, and crucial residues in loops 10−24, 138−148, 160−162, and 224−232 key in binding and orienting G1P and dTTP are also involved in intersubunit contacts (Figure 6). Comparisons of all inhibitor-bound structures we have determined show that the loop structure and tetramer arrangement are essentially unchanged between them. The tetramer arrangement we see in our inhibited complexes is indeed different from that observed in an *E. coli* RmlA-dTTP complex with an empty allosteric site (PDB code 1MC3[14]). (We have been unable to obtain an equivalent *P. aeruginosa* RmlA complex, the ideal comparison point. In our attempts

dx.doi.org/10.1021/cb300426u | *ACS Chem. Biol.* 2013, 8, 387−396

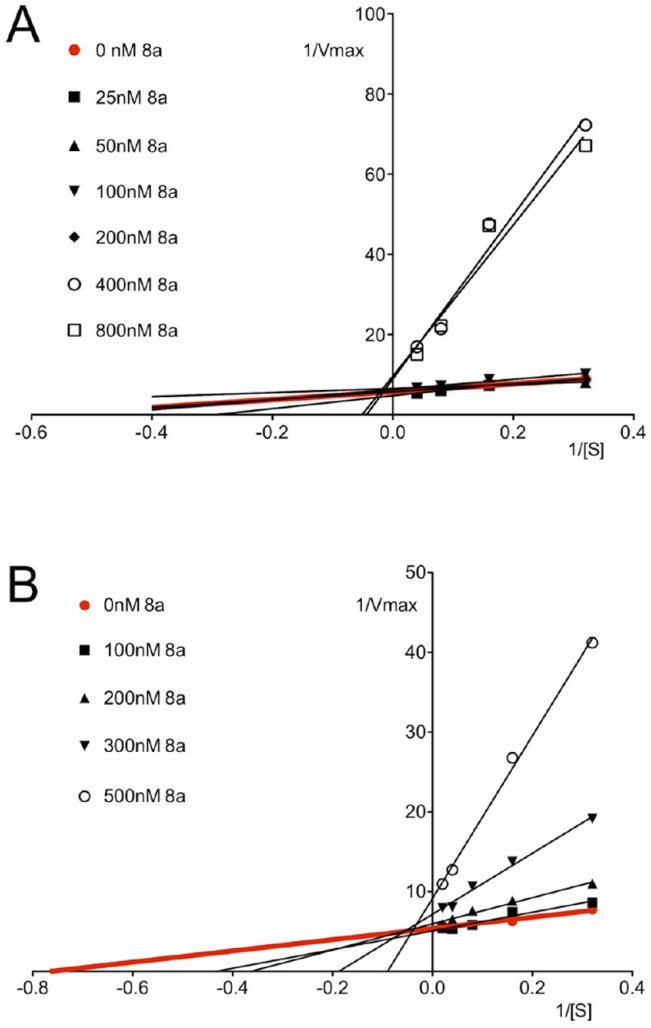

Figure 4. Lineweaver–Burke analysis showing the effects of **8a** on binding of substrates. (A) Compound **8a** has little effect on dTTP binding unless at a very high concentration. (B) Compound **8a** shows competitive inhibition pattern with respect to G1P binding. Controls with no inhibitor are shown as red lines.

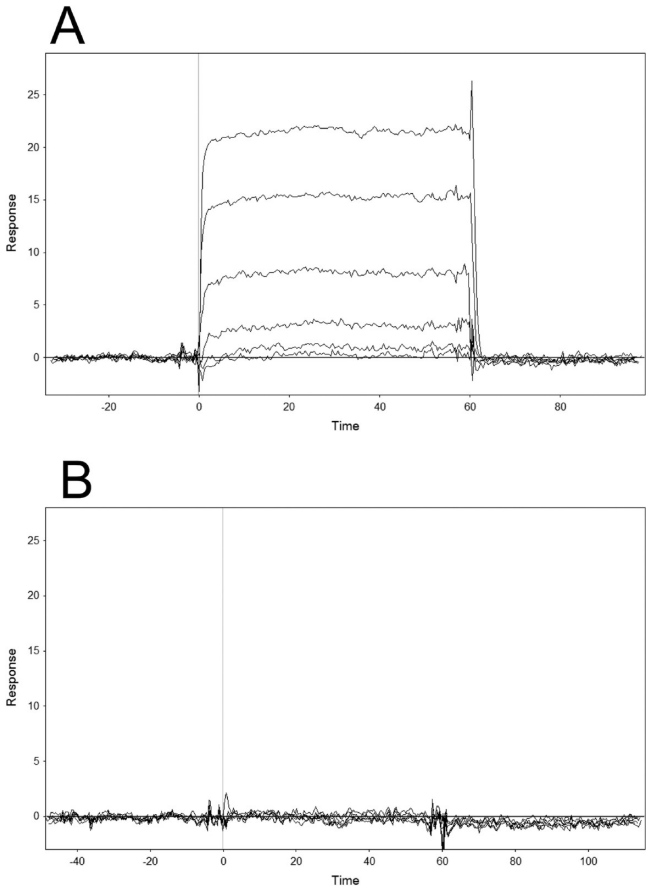

Figure 5. SPR sensorgrams showing substrate interactions with RmlA in the presence of **8a**. (A) dTTP titration in the presence of **8a** and G1P reveals dTTP binds to RmlA with a K_D of 101 μM (95% CI 79–130 μM). (B) G1P titration in the presence of **8a** and dTTP reveals G1P does not bind to the RmlA, thus confirming that **8a** displays competitive inhibition with respect to G1P binding.

both sites are occupied or both empty, resulting in a tetramer arrangement identical to that of the inhibited structures.) The change in the tetramer organization can be magnified by superimposing the structures using only one subunit of each structure (Figure 6). Using this method of superposition, the main chain Arg219 whose side chain inserts into the allosteric site from the other monomer in the inhibited structure (where it makes a monomer–monomer salt bridge as well as stacking with the inhibitor) has shifted over 6 Å in the uninhibited structure. The four C-terminal residues (290–293) that fold back over the allosteric site in the inhibited structure extend into space in the uninhibited structure. The different structure at the C-terminus results in a significant structural shift of the turn at Gln152 in the other monomer. These changes in the monomer–monomer interface are reflected at the dimer–dimer interface where the inhibited structure has a "tighter" packing arrangement. This transmission of structural change from one allosteric binding site across the monomer–monomer interface to the other allosteric site and then across the dimer–dimer interface is we believe the origin of the remarkable cooperativity of inhibitor binding.

At the active site we note, in particular, changes in two regions that are both involved in binding G1P: the side chains of Glu161–Lys162 and the backbone at Tyr145. Both regions are shifted by around 2 Å, creating a larger pocket in the uninhibited structure relative to inhibited. These regions flank the turn at Gln152, which as mentioned previously is sensitive to the changes at the allosteric site. The changes in the loops that bind dTTP between the structures are much less significant, consistent with the lack of inhibition of dTTP binding. We suggest that the inhibitors act by locking the conformational state of the RmlA tetramer and thereby preventing dTTP from inducing the conformational changes necessary to create the G1P binding site.

Conclusion. We report a novel small molecule scaffold that is a potent inhibitor of the first enzyme (RmlA) of the dTDP-L-rhamnose biosynthetic pathway. The pathway is essential for *M. tuberculosis* where the compounds show some biological activity. In a mouse model we have also demonstrated that RmlA is essential for virulence of *P. aeruginosa* PAO1. This compound series seem to work by exploiting a fundamental property of RmlA, that it possesses an allosteric site that acts as the point of control for the biosynthetic pathway. The second site is present in all RmlA enzymes but absent in other members of the nucleotidyl transferase superfamily, for example human glucose-1-phosphate uridylyltransferase.[32] Although the

dx.doi.org/10.1021/cb300426u | *ACS Chem. Biol.* 2013, 8, 387–396

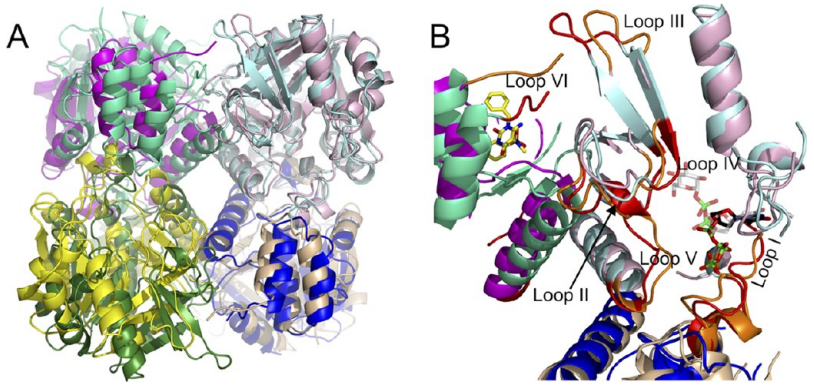

Figure 6. Ribbon diagrams showing the effects on RmlA of having an occupied or empty allosteric site. (A) Overlay of the RmlA-**8a** complex (subunits colored light blue, dark blue, green, and cyan) and *E. coli* RffH (PDB code 1MC3; subunits colored pink, wheat, yellow, and magenta), which has an empty allosteric site. Subunit A from each was overlaid, and the different tetrameric organization can be seen. (B) Close up of the active and allosteric site regions in the overlay. Color scheme as in panel A. The highlighted loops (red for RmlA-**8a**, orange for RffH-dTTP) show the conformational changes that occur between the empty allosteric site and the inhibitor-occupied allosteric site. Loops II and IV form the G1P binding site. The loops correspond to the following residues: I = 10−24; II = 138−148; III = 150−157; IV = 160−162; V = 224−232; VI = 290−293. The substrate dTTP from 1MC3 is shown in black sticks (phosphates in green, oxygens in red), and an overlay of the product dTDP-glucose from 1H5T is shown as white sticks (phosphates in green, oxygens in red) to indicate the binding region in the active site. Inhibitor **8a** is shown as yellow sticks (nitrogens in blue, oxygens in red, and sulfur in orange).

compounds are clearly related to the thymidine ring, they are not identical. Their failure to bind at the active site of RmlA would suggest that they are imperfect mimics of thymidine and thus may not be generally useful against other thymidine sugar-utilizing enzymes.[8] Despite binding remotely from the active site, the inhibitors are competitive with G1P and bind in a highly cooperative manner. Our data suggest this is because they bind at a protein−protein interface, locking the conformation of the protein tetramer and thereby the active site loops. This prevents RmlA from adopting the required conformational change necessary to bind G1P.

METHODS

Cloning, Expression, and Purification. *P. aeruginosa* RmlA was cloned, expressed, and purified based on protocols previously reported by us[33] (see Supporting Information for details). A similar procedure has not yet yielded sufficient amounts of pure RmlA from *M. tuberculosis* for robust *in vitro* assay.

RmlA Hit Identification and Validation. The RmlA high-throughput screen was performed using a Dundee Drug Discovery Unit in-house diverse compound collection of 15,667 molecules. Each assay was performed in a 50 μL reaction volume containing 50 mM Tris, pH 7.4, 5 mM $MgCl_2$, 1 mM dithiothreitol, 0.05% NP-40, 0.1 mM EDTA, 0.1 mM EGTA, 1.5 nM recombinant RmlA, 0.8 μg mL^{-1} pyrophosphatase, 5 μM dTTP, 5 μM G1P, and 30 μM test compound. Test compound was transferred to all assay plates before 25 μL of enzyme mix was added. The reaction was initiated and stopped with the additions of 25 μL of substrate mix and 50 μL of BIOMOL Green, respectively. The assay was run for 30 min at RT, and the BIOMOL Green signal was allowed to develop for 30 min before the absorbance of each well was read at 650 nm. Compounds were designated as hits if the percentage inhibition (PI) was >30% (this value represents 3 standard deviations from the mean data set PI). Preliminary hits were either cherry picked from the original library plates or repurchased. Ten-point inhibitor IC_{50} curves were generated and assays carried out as described in the Supporting Information. All IC_{50} curve fitting was undertaken using ActivityBase XE from IDBS with curves fitted to a four-parameter logistic dose−response curve. All test compound curves had floating top and bottom, and prefit was used for all four parameters.

2D Similarity Screens. 2D similarity searches were run on our in-house database using the Dotmatics browser. Purchased compounds obtained were tested experimentally with results being reported in Table 1 and Supplementary Tables S2 and S3.

Inhibitor Synthesis. All analogues of **1** were prepared according to the protocols supplied in the Supporting Information.

Protein Crystallization. Initial crystallization conditions were found by sparse matrix screening. Precipitant conditions were optimized to 4% PEG 6000, 100 mM MES pH 6.0, 50 mM $MgCl_2$, 100 mM NaBr, and 1% β-mercaptoethanol. Crystals were grown using the sitting drop method with drops comprising 1 μL protein (10 mg mL^{-1}) mixed with 1 μL precipitant. Crystals were grown overnight to dimensions of 0.2 mm × 0.2 mm × 0.1 mm, and cryoprotected in precipitant substituted with 25% glycerol for 5 s, prior to be frozen in a stream of nitrogen gas at 100 K for data collection. Crystallization conditions different from previously published.[33]

Soaking/Co-crystallization. Complexes of RmlA and inhibitor were prepared by soaking or co-crystallization. For soaking, apo-crystals were grown as described in the Supporting Information. Once formed, solid compound was added and left to incubate with the crystals overnight. A selected crystal was then cryo-protected and frozen in a stream of nitrogen gas at 100 K for data collection. For co-crystallization, drops were set up as before, but solid compound was added to the drop prior to sealing and incubation. Crystals typically grew overnight.

Data Collection. Data were processed with iMOSFLM[34] or XIA2[35] incorporating XDS.[36] Each structure was solved using MOLREP,[37] initially using a monomer from 1FZW[15] (apo *P. aeruginosa* RmlA structure), and subsequent complexes using the RmlA-**1** subunit of the complex with the inhibitor removed. Refinement used REFMAC5[38] and statistics shown in Supplementary Tables S1 and S4−S6. Model building was performed using COOT,[39] and ligands built using the PRODRG server.[40] Structural figures were prepared with PyMOL.[41] Ligands were built into difference electron density which was also stronger for the "thymidine-like" ring and weaker for substituents. Occupancy was set to 1 for all atoms in ligand except **4**, where the five-membered ring was modeled in two (0.5 occupancy) positions. The unit cells are different from those in the PDB for other previously reported *P. aeruginosa* complexes. Unbiased maps for each complex are shown in Supplementary Figure S19.

Surface Plasmon Resonance. Binding of analytes (substrates and **8a**) to RmlA was investigated using a Biacore 3000 instrument as described in the Supporting Information.

Kinetic Parameter Determinations. The enzymatic activity of RmlA was determined using a protocol analogous to that described above for the HTS. Michaelis constants for each substrate (dTTP and

G1P) were determined with data fitted to the Michaelis−Menten equation using GraFit. Data sets for each substrate (dTTP and G1P) were also fitted to the Hill equation. Further details are given in the Supporting Information.

***Pseudomonas aeruginosa* RmlA Gene Knockout Virulence Studies.** Wild-type and RmlA knockout mutant strains of *P. aeruginosa* were prepared and used to infect NMRI outbred mice. Bacterial quantification using mouse lung homogenates is detailed in the Supporting Information.

***Mycobacterium tuberculosis* MIC Determination.** MIC values were determined against *M. tuberculosis* (H37Rv) by the microbroth dilution method as described in the Supporting Information.[42]

Accession Codes. Protein Data Bank codes 4ARW (RmlA-**1**), 4AS6 (RmlA-**2**), 4B42 (RmlA-**3**), 4B2X (RmlA-**4**), 4B4B (RmlA-**6**), 4ASJ (RmlA-**8a**), 4ASY (RmlA-**8f**), 4ASP (RmlA-**15a**), 4B3U (RmlA-**12b**), 4B4G (RmlA-**8j**), 4B4M (RmlA-**8k**), 4B5B (RmlA-**8p**).

■ ASSOCIATED CONTENT

Supporting Information

IC_{50} and Hill coefficient determination of **1** and **2**; data collection and refinement statistics; enzyme−inhibitor interaction schematics; structural overlays; RmlA-knockout in mice; MIC values in *M. tuberculosis*; K_m determination; SPR binding data; unbiased $F_o - F_c$ maps for each ligand; Methods details; synthesis of inhibitors; NMR spectra of inhibitors from Table 1. This material is available free of charge *via* the Internet at http://pubs.acs.org.

■ AUTHOR INFORMATION

Corresponding Author

*E-mail: naismith@st-andrews.ac.uk; njw3@st-andrews.ac.uk.

Author Contributions

[+]These authors contributed equally to this work.

Notes

The authors declare no competing financial interest.

■ ACKNOWLEDGMENTS

The authors wish to thank the Diamond Light Source staff for assistance with data collection and K. Barrack for assistance with ITC. This work was supported by grants from the European Community's Seventh Framework Programme (Aeropath; grant agreement no. 223461), The Scottish Universities Life Science Alliance (L.P., Ph.D. studentship) and the Royal Society (N.W., URF Fellowship).

The coordinates of the RmlA complexes have been deposited in the Protein Data Bank.

■ REFERENCES

(1) Strateva, T., and Yordanov, D. (2009) *Pseudomonas aeruginosa*−a phenomenon of bacterial resistance. *J. Med. Microbiol. 58*, 1133−1148.

(2) Livermore, D. M. (1984) Penicillin-binding proteins, porins and outer-membrane permeability of carbenicillin-resistant and -susceptible strains of *Pseudomonas aeruginosa*. *J. Med. Microbiol. 18*, 261−270.

(3) Livermore, D. M. (2001) Of Pseudomonas, porins, pumps and carbapenems. *J. Antimicrob Chemother. 47*, 247−250.

(4) Hirsch, E. B., and Tam, V. H. (2010) Impact of multidrug-resistant *Pseudomonas aeruginosa* infection on patient outcomes. *Expert Rev. Pharmacoecon. Outcomes Res. 10*, 441−451.

(5) Page, M. G., and Heim, J. (2009) Prospects for the next anti-Pseudomonas drug. *Curr. Opin. Pharm. 9*, 558−565.

(6) LoBue, P. (2009) Extensively drug-resistant tuberculosis. *Curr. Opin. Infect. Dis. 22*, 167−173.

(7) World Health Organisation (2011) *Towards universal access to diagnosis and treatment of multidrug-resistant and extensively drug-resistant tuberculosis by 2015*, pp 1−119, WHO, Geneva.

(8) Singh, S., Phillips, G. N., Jr., and Thorson, J. S. (2012) The structural biology of enzymes involved in natural product glycosylation. *Nat. Prod. Rep. 29*, 1201−1237.

(9) Qu, H., Xin, Y., Dong, X., and Ma, Y. (2007) An rmlA gene encoding d-glucose-1-phosphate thymidylyltransferase is essential for mycobacterial growth. *FEMS Microbiol. Lett. 275*, 237−243.

(10) Li, W., Xin, Y., McNeil, M. R., and Ma, Y. (2006) rmlB and rmlC genes are essential for growth of mycobacteria. *Biochem. Biophys. Res. Commun. 342*, 170−178.

(11) Babaoglu, K., Page, M. A., Jones, V. C., McNeil, M. R., Dong, C., Naismith, J. H., and Lee, R. E. (2003) Novel inhibitors of an emerging target in Mycobacterium tuberculosis; substituted thiazolidinones as inhibitors of dTDP-rhamnose synthesis. *Bioorg. Med. Chem. Lett. 13*, 3227−3230.

(12) Mills, J. A., Motichka, K., Jucker, M., Wu, H. P., Uhlik, B. C., Stern, R. J., Scherman, M. S., Vissa, V. D., Pan, F., Kundu, M., Ma, Y. F., and McNeil, M. (2004) Inactivation of the mycobacterial rhamnosyltransferase, which is needed for the formation of the arabinogalactan-peptidoglycan linker, leads to irreversible loss of viability. *J. Biol. Chem. 279*, 43540−43546.

(13) Sivendran, S., Jones, V., Sun, D., Wang, Y., Grzegorzewicz, A. E., Scherman, M. S., Napper, A. D., McCammon, J. A., Lee, R. E., Diamond, S. L., and McNeil, M. (2010) Identification of triazinoindol-benzimidazolones as nanomolar inhibitors of the Mycobacterium tuberculosis enzyme TDP-6-deoxy-D-xylo-4-hexopyranosid-4-ulose 3,5-epimerase (RmlC). *Biorg. Med. Chem. 18*, 896−908.

(14) Sivaraman, J., Sauve, V., Matte, A., and Cygler, M. (2002) Crystal structure of *Escherichia coli* glucose-1-phosphate thymidylyltransferase (RffH) complexed with dTTP and Mg2+. *J. Biol. Chem. 277*, 44214−44219.

(15) Blankenfeldt, W., Asuncion, M., Lam, J. S., and Naismith, J. H. (2000) The structural basis of the catalytic mechanism and regulation of glucose-1-phosphate thymidylyltransferase (RmlA). *EMBO J. 19*, 6652−6663.

(16) Kim, H., Choi, J., Kim, T., Lokanath, N. K., Ha, S. C., Suh, S. W., Hwang, H. Y., and Kim, K. K. (2010) Structural basis for the reaction mechanism of UDP-glucose pyrophosphorylase. *Molecules Cells 29*, 397−405.

(17) Melo, A., and Glaser, L. (1965) The nucleotide specificity and feedback control of thymidine diphosphate D-glucose pyrophosphorylase. *J. Biol. Chem. 240*, 398−405.

(18) Barton, W. A., Lesniak, J., Biggins, J. B., Jeffrey, P. D., Jiang, J., Rajashankar, K. R., Thorson, J. S., and Nikolov, D. B. (2001) Structure, mechanism and engineering of a nucleotidylyltransferase as a first step toward glycorandomization. *Nat. Struct. Biol. 8*, 545−551.

(19) Barton, W. A., Biggins, J. B., Jiang, J., Thorson, J. S., and Nikolov, D. B. (2002) Expanding pyrimidine diphosphosugar libraries via structure-based nucleotidylyltransferase engineering. *Proc. Natl. Acad. Sci. U.S.A. 99*, 13397−13402.

(20) Williams, G. J., Yang, J., Zhang, C., and Thorson, J. S. (2011) Recombinant E. coli prototype strains for in vivo glycorandomization. *ACS Chem. Biol. 6*, 95−100.

(21) Cid, J. M., Duvey, G., Tresadern, G., Nhem, V., Furnari, R., Cluzeau, P., Vega, J. A., de Lucas, A. I., Matesanz, E., Alonso, J. M., Linares, M. L., Andres, J. I., Poli, S. M., Lutjens, R., Himogai, H., Rocher, J. P., Macdonald, G. J., Oehlrich, D., Lavreysen, H., Ahnaou, A., Drinkenburg, W., Mackie, C., and Trabanco, A. A. (2012) Discovery of 1,4-disubstituted 3-cyano-2-pyridones: a new class of positive allosteric modulators of the metabotropic glutamate 2 receptor. *J. Med. Chem. 55*, 2388−2405.

(22) Trabanco, A. A., Cid, J. M., Lavreysen, H., Macdonald, G. J., and Tresadern, G. (2011) Progress in the developement of positive allosteric modulators of the metabotropic glutamate receptor 2. *Curr. Med. Chem. 18*, 47−68.

(23) Barda, D. A., Wang, Z. Q., Britton, T. C., Henry, S. S., Jagdmann, G. E., Coleman, D. S., Johnson, M. P., Andis, S. L., and Schoepp, D. D. (2004) SAR study of a subtype selective allosteric potentiator of metabotropic glutamate 2 receptor, N-(4-phenox-

yphenyl)-N-(3-pyridinylmethyl)ethanesulfonamide. *Bioorg. Med. Chem. Lett. 14*, 3099−3102.
(24) Gill, J. K., Dhankher, P., Sheppard, T. D., Sher, E., and Millar, N. S. (2012) A series of alpha7 nicotinic acetylcholine receptor allosteric modulators with close chemical similarity but diverse pharmacological properties. *Mol. Pharmacol. 81*, 710−718.
(25) Kessl, J. J., Jena, N., Koh, Y., Taskent-Sezgin, H., Slaughter, A., Feng, L., de Silva, S., Wu, L., Le Grice, S. F., Engelman, A., Fuchs, J. R., and Kvaratskhelia, M. (2012) Multimode, cooperative mechanism of action of allosteric HIV-1 integrase inhibitors. *J. Biol. Chem. 287*, 16801−16811.
(26) Christopoulos, A. (2002) Allosteric binding sites on cell-surface receptors: novel targets for drug discovery. *Nat. Rev. Drug Discovery 1*, 198−210.
(27) Lewis, J. A., Lebois, E. P., and Lindsley, C. W. (2008) Allosteric modulation of kinases and GPCRs: design principles and structural diversity. *Curr. Opin. Chem. Biol. 12*, 269−280.
(28) Brenk, R., Schipani, A., James, D., Krasowski, A., Gilbert, I. H., Frearson, J., and Wyatt, P. G. (2008) Lessons learnt from assembling screening libraries for drug discovery for neglected diseases. *ChemMedChem 3*, 435−444.
(29) Martin, B., Pallen, C. J., Wang, J. H., and Graves, D. J. (1985) Use of fluorinated tyrosine phosphates to probe the substrate specificity of the low molecular weight phosphatase activity of calcineurin. *J. Biol. Chem. 260*, 14932−14937.
(30) Zuccotti, S., Zanardi, D., Rosano, C., Sturla, L., Tonetti, M., and Bolognesi, M. (2001) Kinetic and crystallographic analyses support a sequential-ordered bi bi catalytic mechanism for *Escherichia coli* glucose-1-phosphate thymidylyltransferase. *J. Mol. Biol. 313*, 831−843.
(31) Lafleur, K., Huang, D., Zhou, T., Caflisch, A., and Nevado, C. (2009) Structure-based optimization of potent and selective inhibitors of the tyrosine kinase erythropoietin producing human hepatocellular carcinoma receptor B4 (EphB4). *J. Med. Chem. 52*, 6433−6446.
(32) Yu, Q., and Zheng, X. (2012) The crystal structure of human UDP-glucose pyrophosphorylase reveals a latch effect that influences enzymatic activity. *Biochem. J. 442*, 283−291.
(33) Blankenfeldt, W., Giraud, M. F., Leonard, G., Rahim, R., Creuzenet, C., Lam, J. S., and Naismith, J. H. (2000) The purification, crystallization and preliminary structural characterization of glucose-1-phosphate thymidylyltransferase (RmlA), the first enzyme of the dTDP-L-rhamnose synthesis pathway from *Pseudomonas aeruginosa*. *Acta Crystallogr. Sect. D: Biol. Crystallogr. 56*, 1501−1504.
(34) Leslie, A. G. (2006) The integration of macromolecular diffraction data. *Acta Crystallogr. Sect. D: Biol. Crystallogr. 62*, 48−57.
(35) Winter, G. (2010) xia2: an expert system for macromolecular crystallography data reduction. *J. Appl. Crystallogr. 43*, 186−190.
(36) Kabsch, W. (2010) Xds. *Acta Crystallogr. Sect. D: Biol. Crystallogr. 66*, 125−132.
(37) Vagin, A., and Teplyakov, A. (2010) Molecular replacement with MOLREP. *Acta Crystallogr. D: Biol. Crystallogr. 66*, 22−25.
(38) Murshudov, G. N., Vagin, A. A., and Dodson, E. J. (1997) Refinement of macromolecular structures by the maximum-likelihood method. *Acta Crystallogr. D: Biol. Crystallogr. 53*, 240−255.
(39) Emsley, P., and Cowtan, K. (2004) Coot: model-building tools for molecular graphics. *Acta Crystallogr. D: Biol. Crystallogr. 60*, 2126−2132.
(40) Schuttelkopf, A. W., and van Aalten, D. M. (2004) PRODRG: a tool for high-throughput crystallography of protein-ligand complexes. *Acta Crystallogr. D: Biol. Crystallogr. 60*, 1355−1363.
(41) DeLano, W. L. (2002) The PyMOL Molecular Viewer.
(42) Hurdle, J. G., Lee, R. B., Budha, N. R., Carson, E. I., Qi, J., Scherman, M. S., Cho, S. H., McNeil, M. R., Lenaerts, A. J., Franzblau, S. G., Meibohm, B., and Lee, R. E. (2008) A microbiological assessment of novel nitrofuranylamides as anti-tuberculosis agents. *J. Antimicrob. Chemother. 62*, 1037−1045.